*Laser and Particle Beams* (2012), *30*, 111–116.

doi:10.1017/S0263034611000747

# Effect of plasma material on intense laser-driven beam electrons in solid foils

C.T. ZHOU,[1,2] T.X. CAI,[3] W.Y. ZHANG,[4] AND X.T. HE[1,2]

[1]Institute of Applied Physics and Computational Mathematics, Beijing, People's Republic of China
[2]Center for Applied Physics and Technology, Peking University, Beijing, People's Republic of China
[3]Graduate School of China Academy of Engineering Physics, Beijing, People's Republic of China
[4]China Academy of Engineering Physics, Beijing, People's Republic of China

(RECEIVED 12 October 2011; ACCEPTED 31 October 2011)

**Abstract**

The electromagnetic field structures and transport properties of laser produced relativistic beam electrons propagating through $Au^{+25}$, $Cu^{+20}$, $Al^{+10}$, and $C^{+5}$ plasma foils are investigated. Simulations show that high plasma resistivity as well as high collision rate of the beam electrons with gold and copper plasmas can hinder the forward motion of the beam electrons inside the targets. However, the beam electrons can propagate for a relatively long distance in aluminum and carbon plasma targets. They are well collimated by the strong self-generated resistive magnetic field, resulting in higher sheath electric fields behind the target. The use of low-*Z* target material is therefore more efficient for collimating beam electrons as well as generating higher-energy ions.

**Keywords:** Effect of materials; Laser produce relativistic beam electrons; Solid density plasmas

## INTRODUCTION

Generation and transport of relativistic electrons driven by intense short-pulse lasers are of special interest to many applications in high energy density physics (Cai *et al.*, 2009; Gibbon, 2005; Hoffmann, 2008; Hora, 1988, 2009; Malka *et al.*, 2008; Tahair & Hoffmann, 2009; Sadighi-Bonabi *et al.*, 2010; Wang *et al.*, 2009; Wilks & Kruer, 2000; Wu *et al*, 2009; Yu *et al.*, 2003, 2009; Zhou *et al.*, 2008, 2011), including astrophysics, radiography, medicine, material science, electron and proton acceleration, fast ignition in inertial confinement fusion, etc. Experiments and simulations on the transport of hot electrons in solid-density metallic and plastic targets (Borghesi *et al.*, 1999; Storm *et al.*, 2009) found that the transport and heating properties of hot electrons depend strongly on the electrical resistivity of the plasma materials. Early experiments employing multi-terawatt lasers suggest the use of low-*Z* targets for better collimation of the fast electrons. Simulations (Pukhov & Mayer-ter-Vehn, 1997; Ruhl *et al.* 1999) showed that the magnetic fields formed at the edge of the electron beam in the target tend to collimate the beam electrons. However, recent experiments and simulations found that laser-driven fast electrons in high-*Z* plasmas are not well collimated. Optical imaging, shadowgraphy, and $K_\alpha$ imaging (Lancaster *et al.*, 2007; Robinson & Sherlock, 2007; Green *et al.*, 2008; Zhou *et al.*, 2009, 2010*a*; Wu *et al.*, 2010) showed 30° to 60° beam divergence at laser intensities of $10^{18}$ to $10^{21}$ W/cm$^2$. Since the electric current of relativistic electrons driven by an intense laser pulse can reach 1 GA, the electron streams are subject to two-stream, Weibel, and filamentation, etc. instabilities. Particle-in-cell (PIC) simulations (Birdsall & Langdon, 1985; Silva *et al.*, 2002; Zhou *et al.*, 2009; Wu *et al.*, 2010) indicate that the electron divergence is due to deflection of electrons by the magnetic field associated with filamentation of the electron beam as it propagates through the target.

Collective interaction (Hora, 2009; Storm *et al.*, 2009) of a relativistic electron beam with plasmas of different material can lead to very different dynamic behavior. Theoretically, the self-generated edge magnetic field of the beam formed inside the high-*Z* target is larger than that inside the low-*Z* foil. Large edge magnetic fields would be more efficient to collimate the beam electrons. However, there are other mechanisms affecting the propagation of the beam electrons in overdense plasmas. In this work, we present a comparison of the transport property and electromagnetic field structure of laser produced relativistic beam electrons propagating in gold, copper, aluminum, and carbon plasma foils.

Address correspondence and reprint requests to: C.T. Zhou, Institute of Applied Physics and Computational Mathematics, Beijing 100094, People's Republic of China. E-mail: zcangtao@iapcm.ac.cn

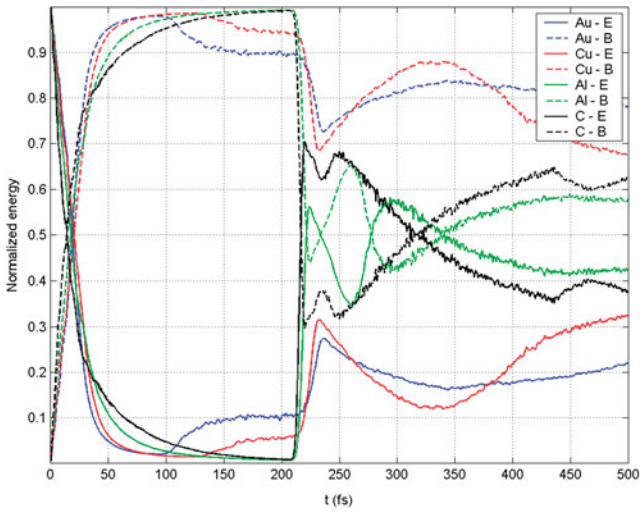


**Fig. 1.** (Color online) The normalized electric and magnetic energies for four plasma materials ($Au^{+25}$, $Cu^{+20}$, $Al^{+10}$, and $C^{+5}$). The peak structures of the electric field energy for the four target materials correspond to $t \approx 237$, 232, 224, and 220 fs, respectively.

We show clearly that high collision rate of the beam electrons with the background plasma and the large space-charged field appearing inside the high-$Z$ target can scatter and prevent the forward propagation of beam electrons.

## LASER-DRIVEN BEAM-ELECTRONS PROPAGATING IN FOUR PLASMA TARGETS

In order to enhance the materials effect, we shall consider four plasma targets, namely $Au^{+25}$ (case I), $Cu^{+20}$ (case II), $Al^{+10}$ (case III), and $C^{+5}$ (case IV). The initial temperature of the plasma electrons and ions is 100 eV. The plasma electron number densities for the four cases are $n_e$ [$cm^{-3}$] = $1.5 \times 10^{24}$, $1.2 \times 10^{24}$, $6 \times 10^{23}$, $3 \times 10^{23}$, respectively. The laser-produced electrons are assumed to satisfy relativistic Maxwellian distribution with an average temperature of 1.5 MeV in the $x$ direction (Solodov *et al.*, 2009; Zhou *et al.*, 2010*b*). The electron beam with radius 15 μm is injected into the plasma along the $z$ direction with an initial angular spread of 30° at ($z$, $x$) = (20,0) μm. The injected current rises to its maximum value in 20 fs and then remains constant. The maximum current density is $10^{13}$ A/$cm^2$.

To simulate the transport of fast electrons in overdense plasmas, we use hybrid simulation techniques (Welch *et al.*, 2001; Honrubia *et al.*, 2005; Davies, 2003; Evans, 2006; Zhou *et al.*, 2009) with PIC beam electrons and fluid background plasmas. The hybrid scheme relaxes the usual PIC restrictions on the temporal and spatial resolutions. The simulation box ($z$, $x$) is 100 μm × 100 μm. The mesh contains 500 × 500 uniform cells, with four injected beam electrons and up to four hundred plasma particles in each

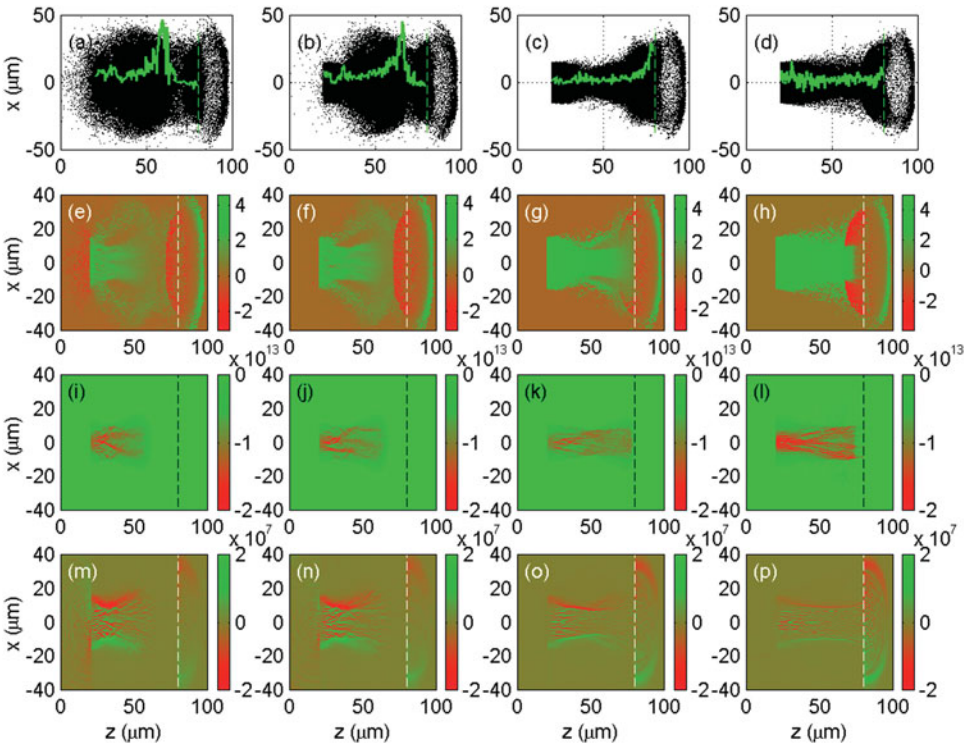


**Fig. 2.** (Color online) Snapshots of the beam-electron behavior and the magnetic field at $t = 267$ fs. (**a**)–(**d**) The phase-space trajectories of the injected beam electrons. (**e**)–(**h**) The intensity distribution $v_z$ of the beam electrons. (**i**)–(**l**) The beam-current density (in A/$cm^2$). (**m**)–(**p**) The magnetic field component $B_y$ (in gauss). The dashed line in all subplots gives the rear surface of the target. The solid line in (a)–(d) shows the $E_z$ profile at $x = 0$, where its value is scaled by $1.5 \times 10^9$ V/m. The first to fourth columns correspond to cases I–IV, respectively.

https://doi.org/10.1017/S0263034611000747 Published online by Cambridge University Press

cell. The temporal resolution is $\delta t = \delta z/2c$ ($c$ is the speed of light in vacuum). The initially uniform plasma slab is located in $20 \le z[\mu m] \le 80$. The vacuum regions are 20 μm both in front of and behind the foil.

The simulation results are summarized in Figures 1–4. Figures 2a, 2e, 2i, and 2m show the injected beam electrons propagating into the gold plasma at $t = 267$ fs. When the beam electrons are injected to the right at ($z = 20$ μm), as can be seen in the phase-space trajectories shown in Figure 2a of the injected beam electrons and their intensity distribution $v_z$ (Fig. 2e), some of the energetic electrons are scattered back from the front surface into the vacuum region. A surface electric field (not shown) is induced to restore neutrality. As the fast electrons enter the gold plasma they set up a charge separation field $\boldsymbol{E} = \eta \boldsymbol{j}_r \approx -\eta \boldsymbol{j}_f$, where η is the plasma resistivity, $\boldsymbol{j}_f$ and $\boldsymbol{j}_r$ are the fast-electron and return currents, respectively. Figure 2a shows that the electric field in the gold plasma can be larger than $10^9$ V/m. In fact, Figure 2a shows that the positive space-charge field can reach $7 \times 10^{10}$ V/m at $z \approx 60$ μm, which decelerates the propagation of the beam electrons. As shown in Figure 2i, the beam current density in the gold plasma can be larger than $10^{13}$ A/cm$^2$. Thus, the beam current far exceeds the Alfvén current and beam transport is possible only if sufficient current neutralization is affected by a return current of background plasma electrons. Further, the Weibel instability leads to break up of the fast electron beam into small beamlets (Weibel, 1995). As shown in Figures 2i and 2m, the beamlets can also coalesce on a longer time scale. The beam electrons deposit their energy to the background plasma through the return current, which can be described by the fluid-electron energy equation (Glinsky, 1995) $\partial T_e/\partial t \approx 2J_r^2/3\sigma n_e$, where σ is the electrical conductivity. Furthermore, non-uniform electric fields can give rise to a large magnetic field $B_y > 10$ MG. Figures 2m and 3a illustrate that $B_y$ component of the magnetic field can reach several tens megagauss. An exponential reduction of the electric field and growth of the magnetic field can be seen in Figure 1, and the fields then saturate before the beam electrons reach the rear surface of the gold target and enter the vacuum. At the rear surface of the target, they generate a strong sheath electric field at $z \approx 80$ μm, as shown in Figure 4a. Once again, the electric field energy can then exponentially increase, as seen in Figure 1.

Figure 1 shows that the first strong peak appears approximately at $t \approx 237$, 232, 224, and 220 fs for the cases I–IV, respectively. It is obvious that hot-electrons propagating in high-$Z$ material targets are slower than in low-$Z$ targets. There are two effects to influence the propagation of beam electrons inside the target. On one hand, the Spitzer

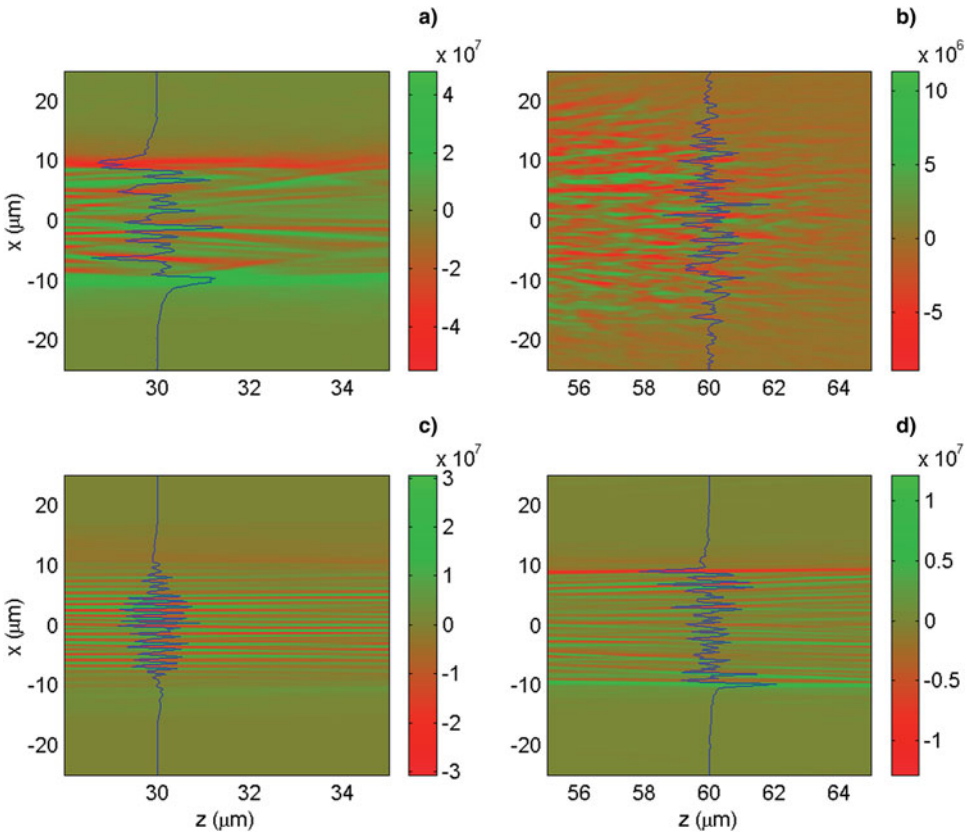


**Fig. 3.** (Color online) Enlargements of the magnetic field $B_y$ (in Gauss) at $t = 267$ fs for $Au^{+20}$ and $C^{+5}$ plasmas, respectively. (**a**) and (**b**) correspond to $Au^{+20}$. (**c**) and (**d**) correspond to $C^{+5}$. The solid lines in the subplots give $B_y$ at $z = 30$ μm (a), (c), and 60 μm (b), (d), respectively.

https://doi.org/10.1017/S0263034611000747 Published online by Cambridge University Press

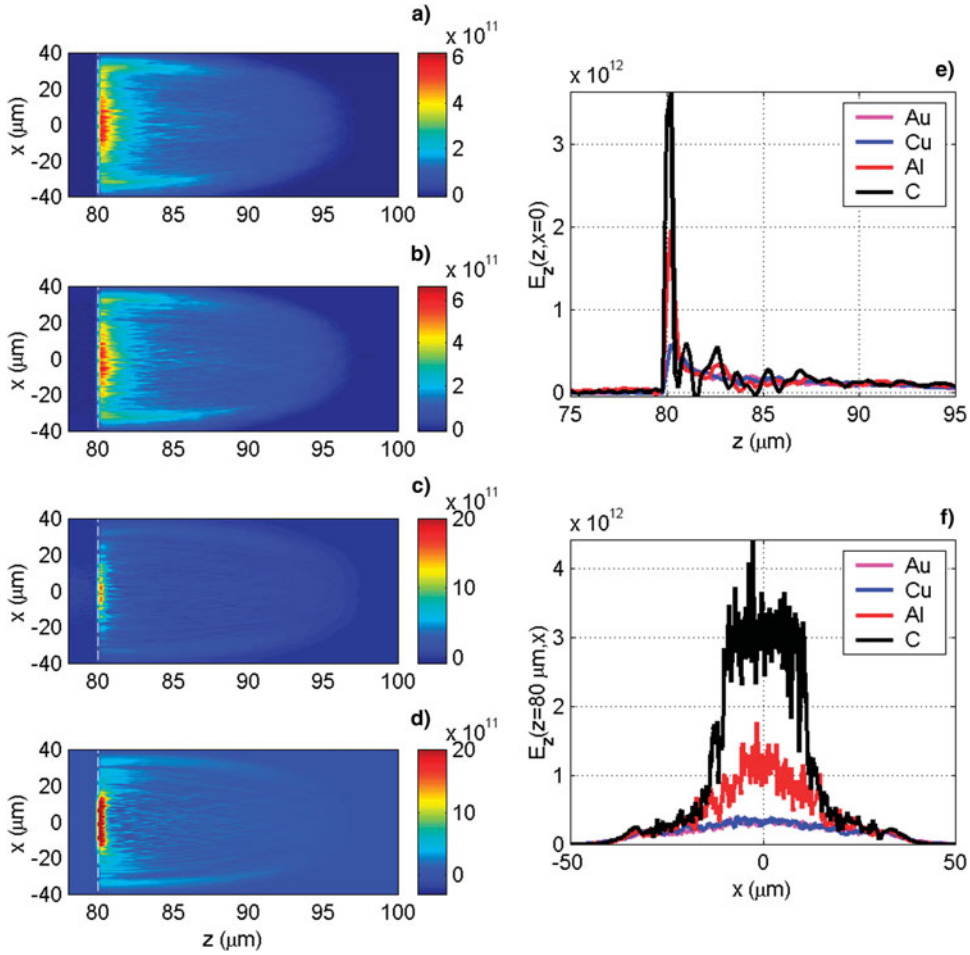


**Fig. 4.** (Color online) Snapshots of the electric field $E_z$ (in V/m) at $t = 267$ fs. (**a**)–(**d**) The electric field structures of near the rear surface correspond to cases I–IV, respectively. (**e**) The electric field profile $E_z$ ($z$) with fixed $x = 0$, and (**f**) $E_z$ ($x$) with fixed $z = 80$ μm.

resistivity $\eta \approx 10^{-2}\, Z \ln \Lambda T^{-3/2}$ (where $\ln \Lambda$ is the Coulomb logarithm) says that the electric field inside high-$Z$ plasma targets by $\boldsymbol{E} = \eta \boldsymbol{j}$ is higher than in low-$Z$ targets, as shown in Figures 2a–2d by the solid line. The large space-charged field appearing inside the high-$Z$ target tend to prevent the forward propagation of beam electrons, as given in Figures 2e–2h. On the other hand, the electron-plasma collision behavior in high-$Z$ cases I and II by $\nu_{e,i} = 4 \times 10^{14}\, Z^2\, (T_e/100\ \text{eV})^{3/2}$ [$\text{s}^{-1}$] can also significantly scatter hot electrons when $n_e > 10^{24}$ $\text{cm}^{-3}$. High collision rate of the beam electron with background plasmas for high-$Z$ cases further slows down the forward propagation of beam electrons. Such stopping/scattering behavior of beam electrons by both electric fields and collision effects can be clearly observed in Figures 2i–2j for corresponding current densities.

The resistive filamentation instabilities associated with the return current of electron beams and/or the self-generated magnetic fields can be seen in Figures 2i–2p. Comparing Figures 2a–2d with 2m–2p, it is seen that the hot-electron beam is sufficiently well collimated in the low-$Z$ foil target (for example, cases III and IV) by the self-generated resistive magnetic field. Inside the target, the magnetic field is mainly generated by the density and resistivity gradients, etc. These two mechanisms can be seen in the magnetic field growth rate (Robinson *et al.*, 2008; Zhou *et al.*, 2011) $\partial \boldsymbol{B}/\partial t \approx \eta \nabla \times \boldsymbol{j} + \nabla \eta \times \boldsymbol{j}$. The observed large magnetic field at the edge of the electron beam or inside the filamentation beam can be associated with the term $\eta \nabla \times \boldsymbol{j}$ due to these electron density and/or velocity fluctuations. In order to compare the difference of resistive magnetic fields for different material plasmas, we in Figure 3 give a comparison of the enhanced magnetic field for the gold (case I) and carbon (case IV) plasmas. At the same initial plasma temperature, we have $\eta_{\text{Au}} > \eta_c$. The edge magnetic field in an early stage formed inside the gold target is larger than that inside the carbon foil, which is clearly observed in Figures 3a and 3c. The large edge magnetic field then focuses the beam electrons. With increasing the propagation distance, the edge magnetic field in case I becomes smaller and smaller (see Fig. 3b) and cannot bend all beam electrons. As shown in Figure 2a, parts of the injected electrons can escape or be scattered into the region $|x| > 15$ μm. However, the edge magnetic field for case IV is still large enough (>10 MG, as seen in Fig. 3d) to narrow the beam divergence. Figures 3a–3b further illustrate

https://doi.org/10.1017/S0263034611000747 Published online by Cambridge University Press

that the filamentation structure can be destroyed by the electron-plasma collision effect inside high-$Z$ targets. For case of low-$Z$ plasma materials, Figures 3c–3d show that regular filamentation beams can be kept for a relatively long distance.

When the beam electrons propagate through the target and enter the rear vacuum, they generate sheath electric field according to the ampere law $\partial \boldsymbol{E}/\partial t = -\boldsymbol{J}$. The sheath electric fields at the rear target surface can be used to diagnose (Ridgers *et al.*, 2011) the distribution of the beam electrons using the relation $n_b \approx -\partial E/ec\partial t$. In other words, the peak value of the longitudinal sheath electric field ($E_z^{\text{peak}}(z)$) can give a description of beam electrons passing through the target rear surface, and the distribution of the transverse electric field ($E_z(x)$) shall show the divergent properties of the injected-electron beam. Figure 4 gives a comparison of the electric field $E_z(x, y)$ for our four cases. In cases I and II, the peak value $E_z^{\text{peak}}(x, y)$ of the sheath electric field is lower that $6 \times 10^{11}$ V/m. In cases III and IV, the peak value can reach $3 \times 10^{12}$ V/m. Figures 4e and 4f gives $E_{z,C}^{\text{peak}}/E_{z,Au}^{\text{peak}} > 5$. On the other hand, Figures 4a–4d and 4f clearly show that the transverse electric fields $E_z(x)$ for our four cases are completely different. Because large edge magnetic fields of the beam in case IV can almost control the beam propagation in the target with an initial radius 15 μm, thus the beam electrons can be concentrated in the rear surface to form a super-Gaussian distribution of the transverse electric field, as shown in Figure 4f. However, in cases I and II, the beam becomes divergent in the target, resulting in the appearance of widen transverse electric field structures. Since sheath field is responsible for proton acceleration from the rear surface, the present results indicate that higher accelerated-proton energy and lower proton emission should occur for the large-scaled carbon target.

## CONCLUSIONS

In conclusion, we have used a two-dimensional hybrid code to investigate the transport and electromagnetic field structures of $Au^{+25}$, $Cu^{+20}$, $Al^{+10}$, and $C^{+5}$ plasma foil targets by relativistic electron beams driven by intense laser pulses. When the relativistic electrons propagate in the targets, the large space-charged field forming inside the highly resistive gold and copper (high-$Z$) targets can greatly hinder the forward propagation of beam electrons, compared to that for the aluminum and carbon (low-$Z$) plasmas. High collision rate of the beam electrons with background plasmas in the high-$Z$ cases can significantly scatter hot electrons, resulting in the destruction of the regular resistive filamentation structure. For low-$Z$ cases, the observed large magnetic field at the edge of the electron beam can bend and collimate most of the beam electrons propagating through the target. By comparing the sheath electric field structure behind the rear surface for different plasma materials, it is found that higher (over five times) sheath electric fields can be generated in the carbon foil than in the gold foil target. The present results clearly suggest that low-$Z$ targets are more favorable for generating higher-energy lower-emission ions (protons) by the target-normal-sheath acceleration mechanism.

## ACKNOWLEDGMENTS

We would like to thank Prof. M. Y. Yu for his useful discussions on this investigation. This work is supported by the National Natural Science Foundation of China, Grant Nos. 10974022 and 10835003, the National Basic Research Program of China (Grant No. 2007CB815101), and the National 863 High-Tech Committee.

## REFERENCES

Birdsall, C.K. & Langdon, A.B. (1985). *Plasma Physics via Computer Simulation*. New York: McGraw-Hill.

Borghesi, M., Mackinnon, A.J. Bell, A.R., Malka, G., Vickers, C., Willi, O., Davies, J.R. Pukhov, A. & Mayer-ter-Vehn, J. (1999). Observations of collimated ionization channels in aluminum-coated glass targets irradiated by ultraintense laser pulses. *Phys. Rev. Lett.* **83**, 4309–4312.

Cai, H.B., Mima, K., Zhou, W.M., Jozaki, T., Nagatomo, H., Sunahara, A. & Mason, R.J. (2009). Enhancing the number of high-energy electrons deposited to a compressed pellet via double cones in fast ignition. *Phys. Rev. Lett.* **102**, 245001 1–4.

Davies, J.R. (2003). Electric and magnetic field generation and target heating by laser-generated fast electrons. *Phys. Rev.* **E68**, 056404–056410.

Evans, R.G. (2006). Modelling short pulse, high intensity laser plasma interactions. *High Energy Density Phys.* **2**, 35–47.

Green, J.S., Ovchinnikov, V.M., Evans, R.G., Akli, K.U., Azechi, H., Beg, F.N., Bellei, C., Freeman, R.R., Habara, H., Heathcote, R., Key, M.H., King, J.A., Lancaster, K.L., Lopes, N.C., Ma, T., Mackinnon, A.J., Markey, K., Mcphee, A., Najmudin, Z., Nilson, P., Onofrei, R., Stephens, R., Takeda, K., Tanaka, K.A., Theobald, W., Tanimoto, T., Waugh, J., Wan Woerkom, L., Woolsey, N.C., Zepf, M., Davies, J.R. & Norreys, P.A. (2008). Effect of laser intensity on fast-electron-beam divergence in solid-density plasmas. *Phys. Rev. Lett.* **100**, 015003 1–4.

Gibbon, P. (2005). *Short Pulse Laser Interactions with Matter – An Introduction*. London: Imperial College Press.

Glinsky, M. (1995). Regimes of suprathemal electron transport. *Phys. Plasmas* **2**, 2796–2806.

Hoffmann, H.H. (2008). Laser interaction with matter and heavy ion fusion. *Laser Part. Beams* **26**, 509–510.

Hora, H. (1988). Particle acceleration by superposition of frequency-controlled laser pulses. *Nature* **333**, 337–338.

Hora, H. (2009). Laser fusion with nonlinear force driven plasma blocks: thresholds and dielectric effects. *Laser Part. Beams* **27**, 207–222.

Honrubia, J.J., Kaluza, M., Schreiber, J., Tsakiris, D. & Meyer-ter-Vehn, J. (2005). Laser-driven fast-electron transport in preheated foil targets. *Phys. Plasmas* **12**, 052708–052716.

Lancaster, K.L., Green, J.S., Hey, D.S., Akli, K.U., Davies, J.R., Clarke, R.J., Freeman, R.R., Habara, H., Key, M.H., Kodama, R., Krushelnick, K., Murphy, C.D., Nakatsutsumi, M., Simpson, P., Stephens, R., Stoeckl, C., Yabuuchi, T., Zepf, M. & Norreys, P.A. (2007). Measurements of energy transport patterns in solid density laser plasma interactions at intensities of $5 \times 10^{20} W\ cm^{-2}$. *Phys. Rev. Lett.* **98**, 125002 1–4.

https://doi.org/10.1017/S0263034611000747 Published online by Cambridge University Press

Malka, V., Faure, J., Gauduel, Y.A., Lefebvre, E., Rousse, A. & Phuoc, K.T. (2008). Principles and applications of compact laser-plasma accelerators. *Nat. Phys.* **4**, 447–453.

Pukhov, A. & Mayer-ter-Vehn, J. (1997). Laser hole boring into over dense plasma and relativistic electron currents for fast ignition of ICF targets. *Phys. Rev. Lett.* **79**, 2686–2689.

Ridgers, C.P., Sherlock, M., Evans, R.G., Robinson, A.P., & Kingham, R.J. (2011). Superluminal sheath-field expansion and fast-electron-beam divergence measurements in laser-solid interactions. *Phys. Rev. **E*** **83**, 036404 1–10.

Robinson, A.P.L. & Sherlock, M. (2007). Magnetic collimation of fast electrons produced by ultraintense laser irradiation by structuring the target composition. *Phys. Plasmas* **14**, 083105 1–7.

Ruhl, H., Macchi, A., Mulser, P., Cornolti & Hain, S. (1999). Collective Dynamics and Enhancement of Absorption in Deformed Targets. *Phys. Rev. Lett.* **82**, 2095 1–4.

Sadighi-Bonabi, B., Hora, H., Riazi, E., Yazdani, E. & Sadighi, S.K. (2010). Generation of plasma blocks accelerated by nonlinear foces from ultraviolet KrF laser pulses for fast ignition. *Laser Part. Beams* **28**, 101–107.

Silva, L.O., Fonseca, R.A., Tonge, J.W., Mori, W.B. & Dawson, J.M. (2002). On the role of the purely transverse Weibel instability in fast igniter scenarios. *Phys. Plasmas* **9**, 2458–2461.

Solodov, A.A., Anderson, K.S., Betti, R., Gotcheva, V., Myatt, J., Delettrez, J.A., Skupsky, S., Theobald, W. & Stoeckl, C. (2009). Integrated simulations of implosion, electron transport, and heating for direct-drive fast-ignition targets. *Phys. Plasmas* **16**, 056309.

Storm, M., Solodov, A.A., Myatt, J.F., Meyerhofr, D.D., Stoeckl, C., Mileham, C., Betti, R., Nilson, P.M., Sangster, T.C., Teheobald, W. & Guo, C. (2009). High-current, relativistic electron-beam transport in metals and the role of magnetic collimation. *Phys. Rev. Lett.* **102**, 235004 1–4.

Tahair, N. A & Hoffmann, D.H.H. (2009). Development of advanced fuel inertial fusion targets. *Laser Part. Beams* **15**, 575–587.

Wang, W.M., Sheng, Z.M. & Zhang, J. (2009). Electron injection into laser wakefields by colliding circularly-polarized laser pulses. *Laser Part. Beams* **27**, 3–7.

Weibel, E.S. (1995). Spontaneously growing transverse waves in a plasma due to an anisotropic velocity distribution. *Phys. Rev. Lett.* **2**, 83–86.

Welch, D.R., Rose, D.V., Oliver, B.V. & Clark, R.E. (2001). Simulation techniques for heavy ion fusion chamber transport. *Nucl. Instrum. Meth. Res.* **A464**, 134–139.

Wilks, S.C. & Kruer, W.L. (2000). Absorption of ultrashort, ultraintense laser light by solids and overdense plasmas. *IEEE J. Quan. Elec.* **33**, 1954–1969.

Wu, S.Z., Zhou, C.T. He, X.T. & Zhu, S.P. (2009). Generation of strong magnetic fields from laser interaction with two-layer targets. *Laser Part. Beams* **27**, 471–474.

Wu, S.Z., Zhou, C.T. & Zhu, S.P. (2010). Effect of density profile on beam control of intense laser-generated fast electrons. *Phys. Plasmas* **17**, 063103 1–7.

Yu, M.Y., Yu, W., Chen, Z.Y. Zhang, J., Yin, Y., Cao, L.H., Lu, P.X. & Xu, Z.Z. (2003). Electron acceleration by an intense short-pulse laser in underdense plasma. *Phys. Plasmas* **10**, 2468–2474.

Yu, W., Cao, L., Yu, M.Y., Cai, H., Xu, H., Yang, X., Lei, A., Tanaka, K.A. & Kodama, R. (2009). Plasma channeling by multiple short-pulse lasers. *Laser Part. Beams* **27**, 109–114.

Zhou, C.T., He, X.T. & Yu, M.Y. (2008). Laser-produced energetic electron transport in overdense plasmas by wire guiding. *Appl. Phys. Lett.* **92**, 151502 1–3.

Zhou, C.T., He, X.T., Cao, J.M., Wang, X.G. & Wu, S.Z. (2009). Reducing current loss of laser-driven fast electron beams propagating in solid-density plasmas. *J. Appl. Phys.* **105**, 105, 0833111–7.

Zhou, C.T., Wang, X.G., Wu, S.Z., Cai, H.B., Wang, F. & He, X.T. (2010*a*). Density effect on relativistic electron beams in a plasma fiber. *Appl. Phys. Lett.* **97**, 051502 1–3.

Zhou, C.T., Wu, S.Z., Cai, H.B., Chen, M., Cao, L.H., Chew, L.Y. & He, X.T. (2010*b*). Hot electron transport and heating in dense plasma core by hollow guiding. *Laser Part. Beams* **28**, 563–570.

Zhou, C.T., He, X.T. & Chew, L.Y. (2011). Intense short-pulse lasers irradiating wire and hollow plasma fibers. *Opt. Lett.* **36**, 924–926.

https://doi.org/10.1017/S0263034611000747 Published online by Cambridge University Press